Title

Cerebral structure on magnetic resonance imaging in language- and learning-impaired children.

Journal

Archives of neurology, 48(5)

ISSN

0003-9942

Authors

Jernigan, TL
Hesselink, JR
Sowell, E
et al.

Publication Date

1991-05-01

DOI

10.1001/archneur.1991.00530170103028

Peer reviewed

Cerebral Structure on Magnetic Resonance Imaging in Language- and Learning-Impaired Children

Terry L. Jernigan, PhD; John R. Hesselink, MD; Elizabeth Sowell; Paula A. Tallal, PhD

• **Using magnetic resonance imaging 20 language- and learning-impaired children were compared with 12 normal control subjects. Gross brain structure was remarkably normal in the language- and learning-impaired group. Semiautomated morphometry was used to measure hemispheric volumes and cerebral asymmetries in six cerebral regions. The volume of the left posterior perisylvian region was significantly reduced in language- and learning-impaired children. Asymmetries in inferoanterior and superoposterior cerebral regions were also significantly different in this group. Results of descriptive group comparisons of estimated volumes of other cerebral gray-matter structures raise the possibility that some language- and learning-impaired children may have additional volume reductions in cortical and subcortical structures. The results suggest that hemispheric specialization of function may be anomalous in this population.**

(*Arch Neurol.* 1991;48:539-545)

Developmental dysphasia is a specific disorder of language development of unknown etiology.[1] Because the disorder is not life-threatening, neuropathological examinations have been reported in only a few cases.[2,3] Neuropathological studies of dyslexia, a closely related developmental disorder of reading,[4,5] have led to hypotheses about its pathogenesis.[6] Symmetry of the planum temporale of the posterotemporal lobe, an unusual finding in normal subjects, was noted in all dyslexic patients examined in these studies. Also observed were frequent ectopias and dysplasias of the cortex. The planum symmetry appeared to be associated with larger right plana, rather than smaller left plana. It was hypothesized that injury to the brain during corticogenesis may lead to enhanced survival of right planum neurons, which produces anatomical symmetry and altered cerebral dominance.

With the recent advent of noninvasive, in vivo brain imaging methods, a few studies of dyslexia have been reported[7-10] (reviewed by Hynd and Semrud-Clikeman[11]). These imaging studies, employing several different measurement techniques, generally support neuropathological findings of unusual patterns of hemispheric asymmetry in dyslexic subjects. Of the new imaging techniques, magnetic resonance imaging (MRI) offers the most sensitive, noninvasive method for assessing brain structure during life and, as such, provides an unique opportunity for examining brain structure in children with specific developmental language disabilities.

In this study, MRI images from 20 language- and learning-impaired (L/LI) children and 12 matched control subjects were analyzed with semiautomated brain morphometry. Estimated volumes were obtained of cerebral regions and individual gray-matter structures. Based on previous findings with dyslexic children, specific analyses were developed to determine whether L/LI children would show anomalous asymmetries relative to controls.

SUBJECTS AND METHODS

The sample studied was drawn from a larger sample of 95 specifically language-impaired children and 60 age-, IQ-, race-, and socioeconomic status–matched controls, identified at the age of 4 years and studied longitudinally until the age of 8 years. Inclusion in the longitudinal study at the age of 4 years was based on the following criteria for both groups: (1) performance IQ of 85 or greater; (2) normal hearing acuity, no motor handicaps, and no oral, structural, or motor impairments affecting nonspeech movement of the articulators; (3) an English language background without significant dialectical or language differences in the home environment; (4) no obvious signs of infantile autism (as defined by *Diagnostic and Statistical Manual of Mental Disorders, Third Edition*[12]); and (5) no known neurological disorders. Language-impaired children were at least 1 year behind chronological and nonverbal mental age on a battery of standardized receptive and expressive language measures. Normal control children met the same criteria as the language-impaired subjects except that their speech and language skills had to be within 6 months of their chronological age.

A subset of children who completed all 5 years of testing in the longitudinal study were selected to participate in this study. Twenty-eight children who continued to demonstrate significant language impairment as well as academic achievement deficits were selected as L/LI subjects. These subjects were selected initially based on their language impairment at the age of 4 years. At the time of this imaging study, when they had an average age of 9 years, they continued to be language impaired, but in addition, many had severe learning disabilities that emerged during the longitudinal study. For this reason, these subjects have been classified as L/LI. They may or may not be the same as those children selected based solely on reading ability (ie, developmental dyslexics), although they all did have severe reading impairment when MRI scanning was performed. Fourteen matched controls who demonstrated normal language development and academic achievement (reading, spelling, and mathematics) also agreed to participate.

Eight of the L/LI children and two of the controls were unable to complete the procedure, or the magnetic resonance images were

Accepted for publication October 17, 1990.

From the San Diego (Calif) Veterans Affairs Medical Center (Dr Jernigan); the Departments of Psychiatry (Dr Jernigan), Radiology (Drs Jernigan and Hesselink), and Neurosciences (Dr Hesselink), the University of California, San Diego School of Medicine and the Brain Image Analysis Laboratory, University of California, San Diego School of Medicine, La Jolla (Ms Sowell); and the Center for Molecular and Behavioral Neurosciences, Rutgers University, New Brunswick, NJ (Dr Tallal).

Reprint requests to Department of Psychiatry, 0631-P, University of California, San Diego, 9500 Gilman Dr, La Jolla, CA 92093-0631 (Dr Jernigan).

technically inadequate for analysis owing to motion artifact. Thus, 20 L/LI children (13 boys and seven girls) and 12 control children (eight boys and four girls), aged 8 to 10 years, were studied. Table 1 summarizes the subjects' characteristics. The groups remained well matched for age and sex; however, the controls had a somewhat higher mean performance IQ. Seventeen of the L/LI children had Wechsler Intelligence Scale for Children performance IQs greater than 80. The remaining three had performance IQs of 75, 73, and 64 (demonstrating a decrease from their previous performance IQs as measured at the age of 4 years). Also, at the time of MRI scanning, all L/LI children lagged 2 years behind chronological age on the Curtiss-Yamada Comprehensive Language Evaluation Expressive or Receptive scales, except for one child who lagged 1 year behind on both scales, but had mathematics and vocabulary percentile scores of 0.

All but three children (two L/LI, one control) were right-handed. Because of concern about altered cerebral organization and symmetry in the left-handers, all analyses were conducted with and without these subjects. Both sets of results are given below, although they were virtually identical.

Table 1.—Subject Characteristics*

	Control	L/LI
No. of subjects	12 (11)	20 (18)
Sex, F/M	4/8 (3/8)	7/13 (6/12)
Handedness, L/R	1/11 (11)	2/18 (18)
Age, y, mean ± SD	9.0 ± 0.7 (8.9 ± 0.7)	8.9 ± 0.7 (9.0 ± 0.7)
WISC PIQ, mean ± SD	109 ± 14 (110 ± 14)	97 ± 16 (98 ± 16)
CYCLE age levels, mean ± SD		
Expressive	8.3 ± 1.4 (8.2 ± 1.5)	4.8 ± 1.2 (4.7 ± 1.3)
Receptive	8.3 ± 1.0 (8.4 ± 0.9)	5.3 ± 1.4 (5.3 ± 1.4)

*Results omitting left-handed subjects are given in parentheses. L/LI indicates language and learning impaired; WISC PIQ, Wechsler Intelligence Scale for Children Performance IQ; and CYCLE, Curtiss-Yamada Comprehensive Language Evaluation. CYCLE age levels are equivalents at 8-year-old testing. One L/LI subject who did not complete the WISC testing is omitted from the calculation of PIQ; his Leiter IQ was 118 less than 1 year before scanning.

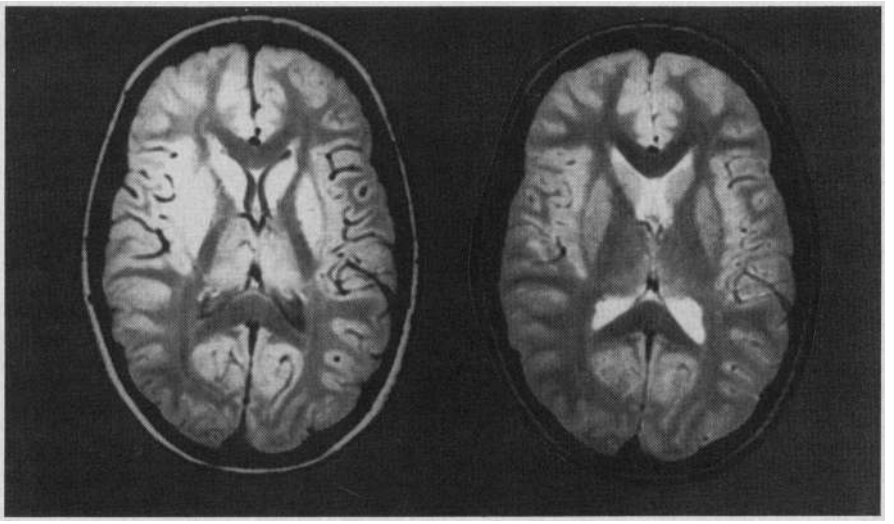

Fig 1.—Representative images from the standard protocol. Left, Repetition time, 2000 milliseconds; echo time, 25 milliseconds (proton density–weighted in text). Right, Repetition time, 2000 milliseconds; echo time, 70 milliseconds (T_2-weighted in text). Sections are 5 mm thick, with 2.5-mm gaps between images. A 24-cm field of view was used, and the matrix was 256 × 256.

MRI Protocol

Magnetic resonance imaging was performed with a 1.5-T superconducting magnet (Signa; General Electric, Milwaukee, Wis) at the University of California, San Diego/AMI Magnetic Resonance Institute. Proton density–weighted and T_2-weighted images (Fig 1) were obtained simultaneously for each section, using an asymmetrical, multiple-echo sequence (repetition time, 2000 milliseconds; echo time, 25, 70 milliseconds) to obtain images of the entire brain in the axial plane. Section thickness was 5 mm, with a 2.5-mm gap between successive sections in all instances. A 256 × 256 matrix and 24-cm field of view were used. Thus, a voxel measured 0.9375 × 0.9375 × 5 mm, subtending a volume of 4.39 mm^3. No sedation was used during these examinations. Informed consent and full cooperation were obtained from all of the children and their parents.

MRI Analysis

The primary goal of the image-analytic methods was to define a region that would include those posterior perisylvian cortical structures of the temporal and parietal lobes that were deemed most relevant for the affected language functions, and to ensure that this region would have consistent boundaries from one subject to the next. Of secondary interest were other regions, including such cortical structures as the anterior language areas in insular cortex and superior parietal association cortex. Finally, for the purpose of exploratory analyses, major subcortical structures were also examined.

The visual identification of specific structures in magnetic resonance images is possible because of the tissue contrast between the gray-matter structures and the surrounding white matter or cerebrospinal fluid (CSF). However, measurements of volumes of cerebral structures must overcome several problems. First, because of partial voluming of gray matter, white matter, and CSF (or all three) at the edges of structures, definite edges are not always present. This allows considerable scope for variability in subjective determinations of such boundaries, for example, when tracing methods are used, leading to measurement unreliability in the computed volumes.

Visual determination of specific cortical structures on MRI depends on the presence of visible gross structural features relative to which the boundaries of the cortical regions can be defined. Standard regional divisions for the cortex are largely based on cortical gyral patterns, but the accurate localization of particular gyri or sulci, throughout a series of images, is often impossible. Furthermore, some boundaries, such as that between posterotemporal and inferoparietal cortex, are not clearly defined in gross structural terms (Fig 2). Also, even when attempts are made to standardize head positioning, head rotation (relative to the imaging plane) occurs in all three planes. This is especially true with unsedated subjects who must be sufficiently comfortable in position to avoid movement during the imaging session. Careful inspection indicates that small rotations substantially change the appearance of brain structures in the image plane, further complicating their visual identification; in addition, such rotations lead to spurious within-plane asymmetries of apparently comparable structures in the two hemispheres. Thus, manually tracing the structures in the sections where they are best visualized often leads to inaccurate volume and asymmetry assessments. The following techniques are designed to address each of these difficulties.

To facilitate and standardize the determination of structural edges, the present method involves a semiautomated classification of all pixels in the images based on their signal characteristics on the two original images of each section. A detailed description of the basic image analysis method has been reported elsewhere.[13] Only a brief summary is provided herein. For each axial brain section imaged, a computed matrix is produced. In this matrix, voxels are classified as most resembling (in signal strength) gray matter, white matter, CSF, or signal hyperintensities (tissue abnormalities). The full series of axial images is analyzed, beginning at the

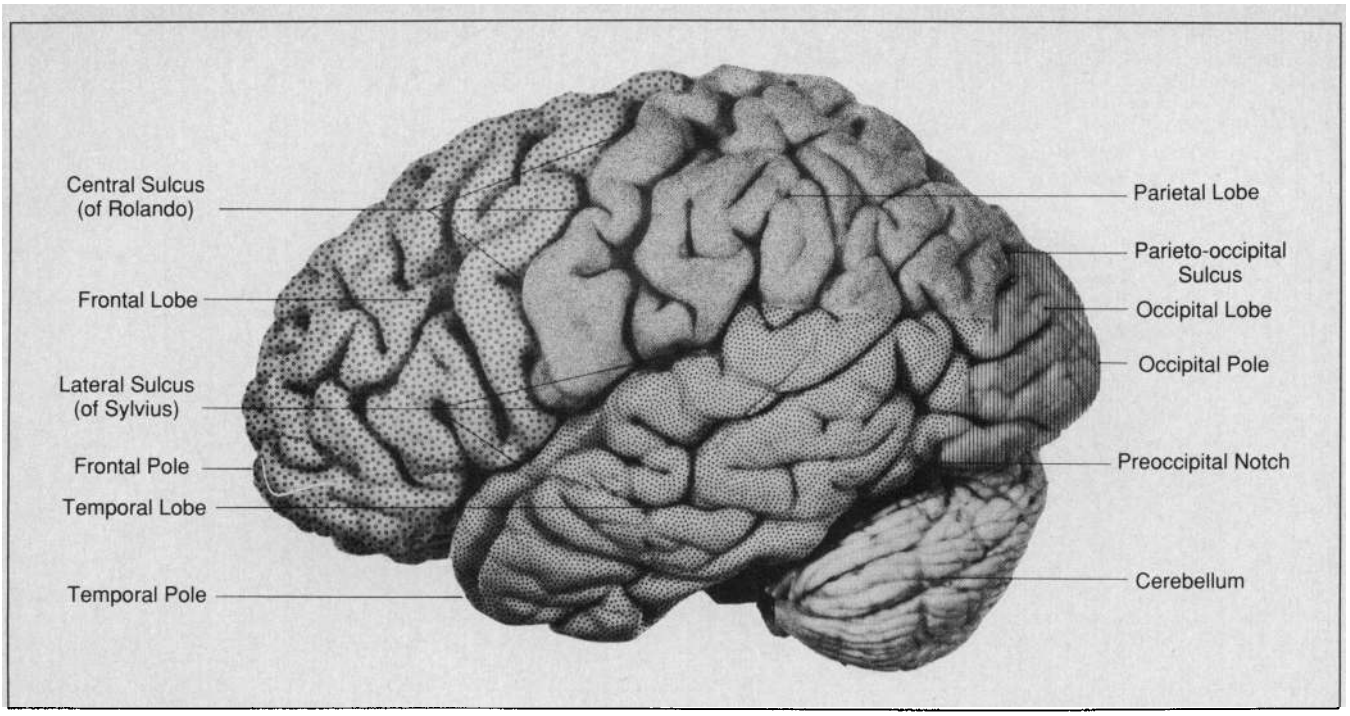

Fig 2.—The lateral surface of the brain (from Montemurro and Bruni[23]). The primary lobes of the cortex are designated by stippling. Gross structural features such as the fissure of Rolando and the sylvian fissure provide partial lobar boundaries on the cortical surface. However, no gross anatomical landmarks are present on the surface of the posterotemporal and inferoparietal lobes to define their boundary, and a somewhat arbitrary line is drawn. The anterior border of the occipital lobe also lacks surface landmarks for precise localization.

bottom of the cerebellar hemispheres and extending through the vertex.

Further manipulations to derive the measures for this study were then made by trained operators, who were "blind" to subject age or group status, using a stylus-controlled cursor on the displayed "pixel-classified" images.

Definition of Subcortical Structures

To delineate subcortical structures, the operators circumscribed pixels classified as gray matter that were visually determined to be in caudate nuclei, lenticular nuclei, and diencephalic gray-matter structures (including mammillary bodies, hypothalamic gray matter, septal nuclei, and thalamus). They did not trace the edges of the structures but defined polygons that included all gray-matter pixels within the structures, and excluded those gray-matter pixels associated with other structures. In some cases, when the subcortical nuclei were contiguous with other areas classified as gray matter but clearly not in the structures, boundaries were manually constructed.

Definition of Cerebral Regions

To define anatomically consistent cerebral regions, a method was adopted for making subdivisions of the cerebrum relative to the centromedial structural midline and two consistently identifiable points: the most anterior midline point in the genu and the most posterior midline point in the splenium of the corpus callosum. By calculating rotation angles using these landmarks, a three-dimensional rotation of the images was performed, thus correcting each individual's image data for rotation out of the optimal imaging plane. Regions could then be constructed that resulted in highly consistent placement of regional boundaries relative to gross anatomical landmarks.

The orientation of the midsagittal plane was first determined by computing a regression line through a series of visually selected brain-stem midline points. The division of the cerebrum was then based on two major planes (Fig 3): an axial plane, which is perpendicular in orientation to the midsagittal plane and parallel to the plane passing through the two corpus callosum points, and a coronal plane, which is defined as perpendicular to the first plane and which passes through the midpoint between the two corpus callosum points. The placement of the axial plane was standardized to the maximum z axis extent of the cerebrum, at 64% of the distance from the bottom of the cerebrum. This distance was chosen because it consistently reached the top of the highest of the two sylvian fissures in a group of eight subjects.

By computing new coordinates for each voxel relative to these planes, each is assigned to one of four zones: one, inferior to the axial plane and anterior to the coronal plane (IA); two, inferior to the axial plane and posterior to the coronal plane (IP); three, superior to the axial plane and anterior to the coronal plane (SA); and four, superior to the axial plane and posterior to the coronal plane (SP). Again, these defined planes are independent of the image plane, as a three-dimensional rotation is first applied based on the positions of the landmarks described earlier. This division resulted in the inclusion of all posterior perisylvian cortical structures in the IP zone; however, the occipital lobe was also included in this zone. Similarly, the IA zone included anterotemporal and frontal cortical structures.

To separate occipital from temporoparietal areas in the IP zone, and prefrontal from anterotemporal areas in the IA zone, two additional coronal dividing planes were defined. In the IA zone, a plane was defined that was parallel to the central plane and passed through the midline genu point. Similarly, in the IP zone, a plane was defined that was parallel to the central plane and that was positioned along the centromedial midline at a distance that consistently fell near the parieto-occipital sulcus. Thus, the two inferior zones were subdivided into four zones, described in gross terms as follows: the first (IA1), the most anterior, included prefrontal cortex; the second (IA2) included anterotemporal and anterior insular cortex; the third (IP1) included posterotemporal, posterior insular, and perisylvian parietal cortex; and the fourth (IP2), the most posterior, included mostly occipital and some posterotemporal cortex on the lateral surface. Figures 3 and 4 illustrate the location of the six cerebral zones defined by these planes. The division of brain structures into the zones is summarized in Table 2.

The regional boundaries are defined relative to the corpus callosum landmarks and the midsagittal plane. Therefore, they do not represent precisely defined neuroanatomical regions. Nevertheless, remarkable consistency in the placement of the boundaries, relative to all recognizable gross features, was observed. Regional maps, such as that seen in Fig 4, were generated for each subject in the study, and each was inspected to

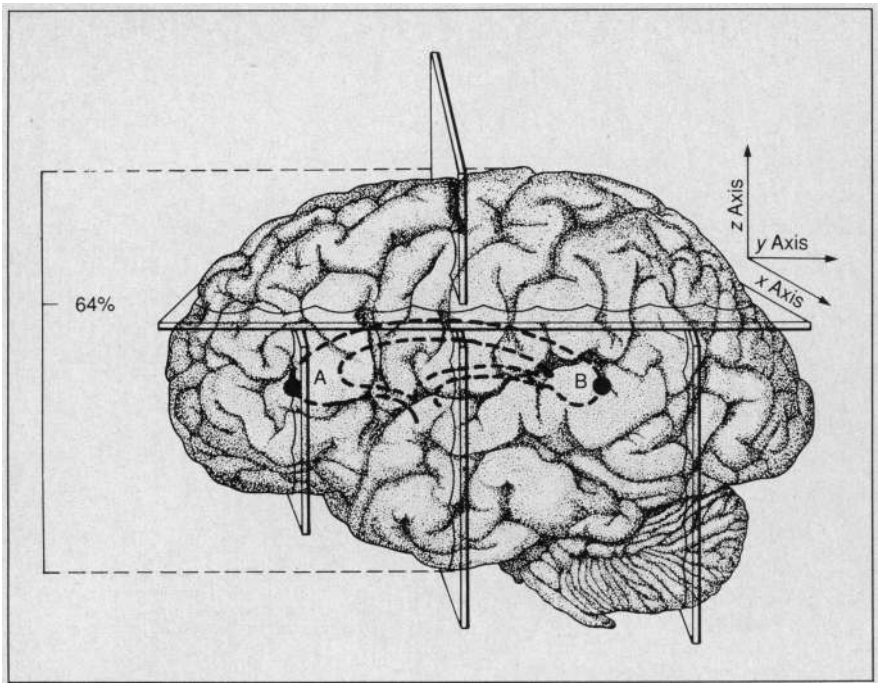

Fig 3.—Cerebral regions are defined as follows. Points A and B in the corpus callosum are the most anterior midline point in the genu and the most posterior midline point in the splenium, respectively. An axial plane, parallel to the plane passing through these two points, is defined as shown, perpendicular to the midsagittal plane. This plane is placed 64% of the distance from the bottom to the top of the supratentorial cranial vault. A coronal plane is defined perpendicular to the axial plane and passing through the midpoint between points A and B. Within the region below the axial dividing plane, two further (parallel) coronal dividing planes are defined, one passing through the genu midline point and one passing through the parieto-occipital sulcus. Thus, six cerebral zones are defined: inferoanterior 1, inferoanterior 2, inferoposterior 1, inferoposterior 2, superoanterior, and superoposterior.

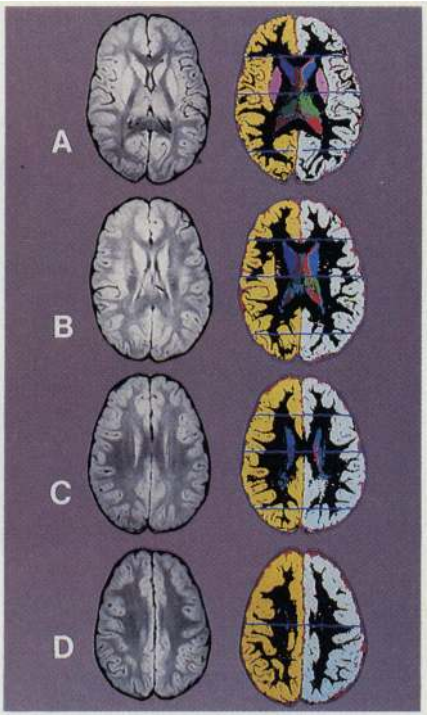

Fig 4.—Representative, fully processed images displayed adjacent to the original proton density–weighted images. Pixels are classified, and zones have been manually designated. The gray-matter pixels have been color coded to display the structural designations: right hemisphere cortical is yellow; left hemisphere cortical, white; caudate, blue; lenticular nucleus, pink; and diencephalon, green. Hyperintense areas within the subcortical regions are shown in gray. Cerebrospinal fluid and white-matter pixels in all regions are displayed in red and black, respectively; however, these pixels are coded so that regional measures may be computed. Sections in A through C are entirely inferior to the axial dividing plane. The section in D is completely superior to the dividing plane. For inferior and superior zones, the central line indicates the position of the major coronal dividing plane. In the inferior zone, two additional lines indicate the positions of the two secondary coronal dividing planes.

ensure that the regions did not vary discernibly in terms of the structures included. In all cases, the inferior zone extended to the highest point in the sylvian fissure that could be recognized in the images. From inspection of the images, Table 2 was compiled to assist in the interpretation of the results. It is not meant to convey the impression that precise boundaries were defined between the structures mentioned.

The total number of supratentorial voxels (including CSF, hyperintensities, and gray and white matter) was computed, by hemisphere, for each of the six zones. Cerebral asymmetry of each of the zones was expressed as a ratio of the left hemisphere measure to its right hemisphere counterpart. Thus, when the left region was larger than the right, the ratio was greater than 1. Volumes of the subcortical gray-matter structures were estimated by summing the appropriate voxels in each hemisphere. All volume estimates are given as simple totals of designated voxels. As described above, each voxel is 4.39 mm^3. However, an estimate of true volume should probably treat the 5-mm sections as representative of the 7.5-mm interslice distance; thus, each voxel would represent 6.49 mm^3. Areas within the lenticular nucleus containing significant iron deposits, particularly in the globus pallidus, do not meet the signal criteria for gray matter and are thus excluded from this region.

A comparison of the original proton density–weighted images and the fully processed images is illustrated in Fig 4. In this figure, the different pixel classes are color coded as follows: right hemisphere cortical gray matter is yellow; left hemisphere cortical gray matter, white; diencephalic areas, green; caudate nuclei, blue; lenticular nuclei, pink; and fluid and white matter, red and black, respectively. Pixels in the subcortical region shown in gray are areas within white matter or surrounding the ventricles that have higher T_2 values than other white matter regions. The blue lines running through the sections indicate the positions of the coronal dividing planes. For this set of images, the boundary between the inferior and superior zones fell between sections C and D.

Statistical Analyses

Group means for the measures were compared with Student's t tests. The comparisons of the six asymmetry measures test the hypothesis that cerebral development is anomalous in the L/LI children. Because of multiple asymmetry comparisons, $P<.01$ was required to reject the null hypothesis. The other comparisons are provided for descriptive purposes only. The meaning of statistical significance of individual test statistics in the context of multiple tests is ambiguous, and probabilities are provided for the secondary comparisons only to aid in interpretation of patterns. Inferences about structural abnormalities from these post hoc comparisons must be made with caution.

RESULTS

On routine clinical neuroradiological evaluation, 16 of 20 examinations in the L/LI children were unremarkable. Slight asymmetry of the ventricles (right larger) was noted in one male subject. One boy and one girl had tiny foci of hyperintensity in deep white matter. In one male participant, bilateral areas of encephalomalacia were present just lateral to the caudate nuclei, with the larger right lesion measuring 8 mm in width.

Among the control children, eight of 12 examinations were unremarkable. Tiny foci of hyperintensity were noted in one boy and one girl. A right cerebellar venous angioma was noted in one boy. A small pituitary gland was noted

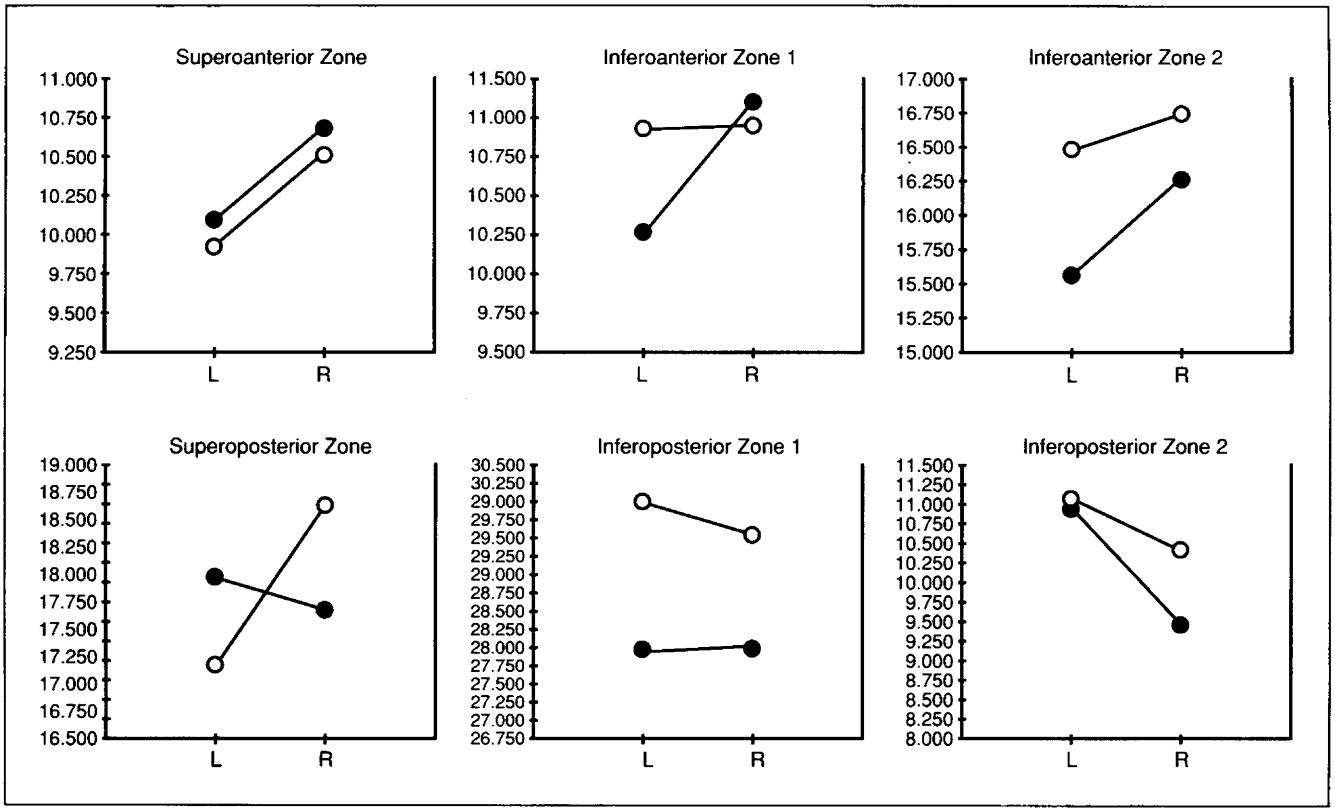

Fig 5.—Mean estimated volumes in thousands of voxels are plotted for each hemisphere by cerebral region. Open circles denote control values; closed circles, values from learning- and language-impaired subjects. All subjects, including left-handers, are included.

Table 2.—Summary of Cortical Structures Within Each Cerebral Region

Inferoanterior 1
Prefrontal cortex inferior to plane above frontal operculum, including orbitofrontal, dorsolateral, and mesial frontal lobe

Inferoanterior 2 (IA2)
Temporal poles, uncus, and some amygdala; anterior perforated substance and adjacent orbitofrontal cortex; anterior insular cortex and frontal operculum

Inferoposterior 1
Most of temporal lobe, including all mesial temporal lobe structures posterior to amygdala (only temporal pole is included in IA2); perisylvian parietal cortex and parietal operculum

Inferoposterior 2
Most of occipital lobe (only small portion of superior occipital cortex is included in SP); small part of most posterior gyri of temporal lobe on lateral cortical surface

Superoanterior
Superior parts of dorsolateral and mesial frontal lobes (above frontal operculum)

Superoposterior (SP)
Superoparietal lobe above parietal operculum; small portion of most superior occipital lobe

Table 3.—Group Differences on Cerebral Asymmetries*

Region	Ratios (L/R) Controls	L/LI	t	P
IA1	1.00 ± 0.04 (1.00 ± 0.04)	0.92 ± 0.07 (0.93 ± 0.06)	3.68 (3.12)	.001 (.004)
IA2	0.99 ± 0.04 (0.98 ± 0.04)	0.96 ± 0.05 (0.97 ± 0.04)	1.66 (1.10)	.107 (.280)
IP1	1.02 ± 0.03 (1.01 ± 0.03)	1.00 ± 0.05 (1.01 ± 0.04)	0.97 (0.30)	.339 (.764)
IP2	1.06 ± 0.10 (1.06 ± 0.10)	1.17 ± 0.16 (1.17 ± 0.16)	2.12 (2.15)	.043 (.041)
SA	0.95 ± 0.10 (0.96 ± 0.09)	0.95 ± 0.07 (0.94 ± 0.06)	0.11 (0.68)	.913 (.503)
SP	0.93 ± 0.07 (0.93 ± 0.08)	1.02 ± 0.08 (1.01 ± 0.07)	3.17 (2.79)	.003 (.010)

*Values are mean ± SD. Results omitting left-handed subjects are given in parentheses. L/LI indicates language and learning impaired; IA1 and IA2, inferoanterior 1 and 2; IP1 and IP2, inferoposterior 1 and 2; SA, superoanterior; and SP, superoposterior.

in another boy. Thus, incidental findings on routine clinical evaluation of the images did not reveal consistent parenchymal or structural differences between the groups.

Group comparisons of cerebral asymmetries in the six regions are summarized in Table 3. The pattern observed only in right-handed subjects is the same as that observed in the full sample. Both IA1 and SP asymmetries are significantly different in the L/LI group ($P<.01$ in each case). The ratio is significantly decreased in the IA1 region and significantly increased in the SP region. An illustration of the different patterns of asymmetry (for the full sample) is provided in Fig 5, showing group mean volumes for the right and left hemispheres within each region. In the normal controls, the IA1 regions are symmetrical, while in the L/LI children, the left hemisphere is reduced relative to the right. For the SP region, the normal controls show right-larger asymmetry, while an opposite pattern is observed in the L/LI subjects.

Secondary analyses focused on the hemispheric volumes of the cerebral (cranial) regions and the subcortical nu-

Table 4.—Group Differences in Cerebral Volumes*

	Volume, Voxels			
	Controls	L/LI	t	P
Cerebral regions				
L IA1	11 125 (11 286)	10 373 (10 277)	1.52 (1.96)	.14 (.06)
R IA1	11 137 (11 361)	11 303 (11 135)	0.27 (0.36)	.79 (.72)
L IA2	16 456 (16 695)	15 539 (15 492)	1.46 (1.86)	.16 (.07)
R IA2	16 693 (16 977)	16 236 (16 069)	0.64 (1.24)	.53 (.23)
L IP1	29 990 (30 163)	27 990 (27 743)	2.18 (2.55)	.04 (.02)
R IP1	29 545 (29 793)	28 032 (27 517)	1.69 (2.77)	.10 (.01)
L IP2	11 027 (10 919)	10 907 (10 559)	0.20 (0.62)	.85 (.54)
R IP2	10 375 (10 343)	9455 (9121)	1.66 (2.37)	.11 (.03)
L SA	9943 (10 073)	10 117 (9976)	0.31 (0.17)	.76 (.87)
R SA	10 527 (10 553)	10 698 (10 693)	0.27 (0.20)	.79 (.84)
L SP	17 231 (17 333)	18 004 (17 615)	1.05 (0.45)	.30 (.66)
R SP	18 650 (18 664)	17 708 (17 549)	1.33 (1.46)	.19 (.16)
Subcortical structures				
L caudate	1031 (1034)	966 (945)	1.61 (2.35)	.12 (.03)
R caudate	1046 (1042)	971 (954)	1.75 (2.08)	.09 (.05)
L lenticular	1257 (1242)	1178 (1171)	1.32 (1.18)	.20 (.25)
R lenticular	1196 (1182)	1126 (1117)	1.19 (1.09)	.24 (.29)
L diencephalic gray	1427 (1411)	1358 (1342)	1.30 (1.28)	.20 (.21)
R diencephalic gray	1439 (1426)	1319 (1301)	2.21 (2.21)	.04 (.04)

*Results omitting left-handed subjects are given in parentheses. Abbreviations are as in Table 3.

Table 5.—Asymmetries in Posterior Perisylvian Region*

	Hemisphere Symmetry (L:R Ratio)		
	R > L (≤0.99)	Symmetrical (0.99-1.01)	L > R (≥1.01)
Controls	1 (1)	4 (4)	7 (6)
L/LI	10 (8)	1 (1)	9 (9)

*Results omitting left-handed subjects are given in parentheses. L/LI indicates language and learning impaired. For total group, Pearson $\chi^2 = 7.9$, $df = 2$, $P = .019$; for group omitting left-handed subjects, Pearson $\chi^2 = 6.5$, $df = 2$, $P = .038$.

clei. Table 4 summarizes group comparisons of these measures. Although many mean volumes are lower in the L/LI group, when examining the full sample, of the cerebral region measures, that in the left IP1 region (posterior perisylvian) is particularly reduced in the L/LI group. Among the subcortical structures, only the right diencephalic volume is notably reduced, although the right caudate measure is also low. The exclusion of left-handers resulted in somewhat larger group differences on these measures, so that left and right IP1 regions appear to be reduced, as is right IP2, and the caudate reductions are slightly more prominent. Though they are not presented herein, no left-right asymmetry in the subcortical volumes yielded a group difference with $P<.05$. Also, because cortical gray-matter volumes were available for right and left hemisphere of each of the six regions, regional cortical asymmetry measures were computed. The pattern of group differences was the same as that for the cranial regions, with significant differences in regions IA1 and SP.

Because earlier studies have classified subjects categorically based on their posterior asymmetries, we examined our data for evidence that the mean asymmetries may have obscured differences in distribution. Indeed, the variance for the asymmetry measures in region IP1 was significantly larger in the L/LI sample than in the control sample ($P<.05$). Therefore, a post hoc frequencies analysis was performed. Table 5 gives the asymmetries in categorical form. The L/LI group did have a somewhat higher prevalence of reversed asymmetries. A χ^2 statistic suggested that the distributions were indeed different; however, the small frequencies in some cells render the statistical test suspect.

Measures of ventricular and sulcal size, as well as proportions of gray to white matter, were similar in the two groups, as assessed with quantitative methods. Furthermore, there was no evidence for abnormal signal values in the white matter in the L/LI children as a group. In summary, there was no evidence from the group comparisons for significant damage to or loss of tissue in the form of increased CSF or hyperintense white matter areas.

COMMENT

The pattern observed in the control subjects of this study suggests that within hemispheres roughly equal in size overall, significant regional asymmetries do occur, with posterior structures larger on the left in inferior and larger on the right in superior zones. In frontal areas, the volumes are symmetrical in the inferior zone, and the right hemisphere volume is larger in the superior zone. The posterior asymmetries seem to be consistent with left hemisphere specialization for language in the posterior temporal lobes and right hemisphere specialization for spatial functions in the parietal lobes. Furthermore, these asymmetries, as well as the frontal asymmetry in the superior zone, are consistent with earlier reports of regional asymmetries in normal subjects.[14-21]

Regarding the absolute values obtained on the asymmetry measures, a caveat should be entered about possible spatial distortion due to field inhomogeneity.[22] Thus, although these results suggest that in both groups the hemispheres are nearly the same size, ie, the left-right ratio has a mean of 0.99 in controls and 1.00 in L/LI children, one or both of the hemispheres may have been systematically measured inaccurately owing to magnification or minification in some parts of the magnetic field. Nevertheless, such factors should have affected both groups similarly.

The L/LI children in this study were selected at 4 years of age because of specific developmental delays in language function in the context of preserved sensory, motor, and nonverbal intellectual capacities. After 5 years of study, at 9 years of age, they have continuing significant, in some cases severe, language and learning impairment. Gross brain structure was remarkably normal in this group of children. There was little evidence for parenchymal damage or volume loss, except in one case. There is definite evidence, however, for anomalous brain development in the form of altered cerebral shape. The L/LI children show abnormal asymmetry, but it does not appear in the posterior perisylvian regions, where it was expected. Rather, these children show an aberrant (right greater than left) asymmetry in the prefrontal region, and an aberrant (left greater than right) asymmetry in the parietal region. Closer inspection of the posterior perisylvian measures, however, reveals a possible explanation for this surprising result. There is evidence from the secondary analyses that this region of the left hemisphere is reduced in volume. Even when this regional volume is expressed as a percentage of the overall supratentorial volume (sum of the regions), it still shows evidence of a proportional decrease in the L/LI children relative to the controls ($P<.05$). However, inspection of the

comparable right hemisphere volume also suggests reduction. Thus, the asymmetry is only slightly affected in this region by the (probably bilateral) volume reduction.

Some earlier imaging studies of developmental language disorders[7,8] have produced evidence of an increased prevalence of reversed asymmetry in posterior hemispheric regions. Such studies generally group the subjects in terms of the direction of their asymmetries. To address these findings directly, we conducted post hoc analyses of the distribution of our posterior perisylvian asymmetries. There was weak statistical evidence that more of the L/LI children showed reversed asymmetry (right greater than left). It, therefore, seems prudent to point out that our results should not be interpreted as refuting the earlier findings and, indeed, they provide some supportive evidence for the presence of more frequent reversals in this region.

The question arises whether the findings in these children are similar to neuropathological results in dyslexic children,[4,5] and whether the anomalous asymmetries in this study could have occurred as a result of the mechanisms hypothesized to account for dyslexia.[6] The planum temporale was not specifically examined in this study, owing to the difficulty of reliably determining its boundaries. Thus, the results do not bear directly on the pathological study results. This structure did always fall within the much larger posterior perisylvian region (IP1), where, although the L/LI children showed more variable asymmetries, no significant mean asymmetry difference was found. The pattern observed in this region might appear to be inconsistent with the reported increase in the size of the right planum in dyslexia. The structures in IP1, including the planum but many others as well, are reduced in volume on the left and are nearly as reduced on the right, relative to controls. Similarly, examination of the pattern within the prefrontal region (IA1), where the L/LI children show greater (right greater than left) asymmetry, suggests that the aberration is more likely to be due to reduction of left structures than to preservation of right structures. In the parietal (SP) region, where the L/LI group shows a reversal of the normal (right greater than left) asymmetry, the right hemisphere is smaller in volume in the L/LI group, while the left is larger, although neither difference is itself statistically significant.

Galaburda and colleagues[4-6] found no evidence for a reduction in neuronal populations in the brains of their dyslexic subjects. Rather, they found evidence for disordered migration and possibly enhanced survival of neurons in critical nondominant hemisphere structures. The subjects examined herein may not be representative of the same population. Although many of them are dyslexic, they were not chosen for isolated reading disorders. Longitudinal study of these children suggests more pervasive linguistic and academic limitations, and evidence indicates that in some children overall intellectual abilities have lagged further and further behind peer standards with increasing age. It is possible that the subjects examined herein suffered effects on neurodevelopment at an earlier stage of neurogenesis, leading to reduced cell populations in critical perisylvian structures (hence, the early prominence of their language disturbances) and ultimately to altered cerebral shape. Interestingly, reduced neuronal populations in left hemisphere insular cortex were noted in one neuropathological study of developmental dysphasia.[3] Even if this explanation is correct, it is still unclear whether the shape alterations observed herein are entirely due to decreased volume of certain affected structures, or if they evolve as early alterations, or exert later effects on mechanisms of cortical maturation and specialization such as those proposed by Galaburda.[6] It is even possible that neuronal loss in related structures may have led to altered maturation of the plana in the subjects of the present study, such that enlarged right plana are present within perisylvian regions that are themselves reduced in volume overall. Perhaps further neuropathological studies in a broader range of developmental disorders may shed some light on these questions.

This study confirms that anomalous neurodevelopment in this disorder does produce structural aberration at a level measurable with in vivo brain imaging. The correlation of such measurements with specific behavioral indices, as development proceeds, may provide some insight into the brain mechanisms involved in developmental cognitive disorders.

This research was supported in part by grant NS22343 from the National Institute of Neurological Disorders and Stroke Multidisciplinary Research Center for the Study of the Neurological Basis of Language, Learning and Behavior Disorders in Children, and by a grant from the Medical Research Service of the Department of Veterans Affairs (Dr Jernigan).

References

1. Benton AL. Developmental aphasia and brain damage. *Cortex*. 1964;1:40-52.
2. Landau WM, Goldstein R, Kleffner FR. Congenital aphasia: a clinicopathological study. *Neurology*. 1960;10:915-921.
3. Cohen M, Campbell R, Yaghmai F. Neuropathological abnormalities in developmental dysphasia. *Ann Neurol*. 1989;25:567-570.
4. Galaburda AM, Kemper TL. Cytoarchitectonic abnormalities in developmental dyslexia: a case study. *Ann Neurol*. 1979;6:94-100.
5. Galaburda AM, Sherman GF, Rosen GD, Aboitiz F, Geschwind N. Developmental dyslexia: four consecutive patients with cortical anomalies. *Ann Neurol*. 1985;18:222-233.
6. Galaburda AM. The pathogenesis of childhood dyslexia. *Res Publ Assoc Res Nerv Ment Dis*. 1988;66:127-137.
7. Hier DB, LeMay M, Rosenberger PB, Perlo VP. Developmental dyslexia. *Arch Neurol*. 1978;35:90-92.
8. Rosenberger PB, Hier DB. Cerebral asymmetry and verbal intellectual deficits. *Ann Neurol*. 1980;8:300-304.
9. Haslam RHA, Dalby JT, Johns RD, Rademaker AW. Cerebral asymmetry in developmental dyslexia. *Arch Neurol*. 1981;38:679-682.
10. Rumsey JM, Dorwart R, Vermess M, Denckla MB, Kruesi MJP, Rapoport JL. Magnetic resonance imaging of brain anatomy in severe developmental dyslexia. *Arch Neurol*. 1986;43:1045-1046.
11. Hynd GW, Semrud-Clikeman M. Dyslexia and brain morphology. *Psychol Bull*. 1989;106:447-482.
12. American Psychiatric Association, Committee on Nomenclature and Statistics. *Diagnostic and Statistical Manual of Mental Disorders, Third Edition*. Washington, DC: American Psychiatric Association, 1980.
13. Jernigan TL, Press GA, Hesselink JR. Methods for measuring brain morphologic features on magnetic resonance images: validation and normal aging. *Arch Neurol*. 1990;47:27-32.
14. Witelson SF, Pallie W. Left hemisphere specialization for language in the newborn. *Brain*. 1973;96:641-646.
15. Wada JA, Clarke R, Hamm A. Cerebral hemispheric asymmetry in humans. *Arch Neurol*. 1975;32:239-246.
16. Chi JG, Dooling EC, Gilles FH. Left-right asymmetries of the temporal speech areas of the human fetus. *Arch Neurol*. 1977;34:346-348.
17. LeMay M. Morphological cerebral asymmetries of modern man, fossil man, and nonhuman primate. *Ann N Y Acad Sci*. 1976;280:349-366.
18. LeMay M, Kido DK. Asymmetries of the cerebral hemispheres on computed tomograms. *J Comput Assist Tomogr*. 1978;2:471-476.
19. Chui HC, Damasio AR. Human cerebral asymmetries evaluated by computed tomography. *J Neurol Neurosurg Psychiatry*. 1980;43:873-878.
20. Geschwind N, Galaburda AM. Cerebral lateralization: biological mechanisms, associations, and pathology, I: a hypothesis and a program for research. *Arch Neurol*. 1985;42:428-459.
21. Bear D, Schiff D, Saver J, Greenberg M, Freeman R. Quantitative analysis of cerebral asymmetries: fronto-occipital correlation, sexual dimorphism, and association with handedness. *Arch Neurol*. 1986;43:598-603.
22. Jack CR, Gehring DG, Sharbrough FW, et al. Temporal lobe volume measurement from MR images: accuracy and left-right asymmetry in normal persons. *J Comput Assist Tomogr*. 1988;12:21-29.
23. Montemurro G, Bruni J. *The Human Brain in Dissection*. 2nd ed. New York, NY: Oxford University Press Inc; 1988:38.